The study of sudden stratospheric warmings using infrasound

Pieter S. M. Smets, Jelle D. Assink, and Läslo G. Evers

Abstract Infrasound has a long history in monitoring SSWs. Several pioneering studies have focused on the various effects of a major warming on the propagation of infrasound, described throughout this chapter. A clear transition can be denoted from observing anomalous signatures towards the use of these signals to study anomalies in upper atmospheric specifications. First studies describe the various infrasonic signatures of a major warming. In general, the significant change in observed infrasound characteristics correspond to summer-like conditions in midwinter. More subtil changes are denoted during a minor warming, recognisable by the presence of a bidirectional stratospheric duct. A combined analysis of all signal characteristic unravels the general stratospheric structure throughout the life cycle of the warming. From then on, infrasound observations are used to evaluate the state of the atmosphere as represented by various NWP models. A new methodology, comparing regional volcano infrasound with simulations using various forecast steps, indicates interesting variations in stratospheric skill.

Assink, Evers, and Smets (e-mail: smets@knmi.nl)
R&D Department of Seismology and Acoustics, Royal Netherlands Meteorological Institute (KNMI), Utrechtseweg 297, 3137 GA De Bilt, The Netherlands

Evers and Smets
Department of Geoscience and Engineering, Faculty of Civil Engineering and Geosciences, Delft University of Technology, Stevinweg 1, 2628 CN Delft, The Netherlands

1 Introduction

Sudden stratospheric warmings (SSWs) are important features of the winter atmosphere (Charlton and Polvani, 2007). During such events, the strongest forcing of the stratosphere on the troposphere is observed (Gerber et al, 2009; Tripathi et al, 2014), influencing weather conditions and its predictability in the troposphere (Jung et al, 2010). Consequentially, improving the predictability of variability in stratosphere, such as SSWs, is important to Numerical Weather Prediction (NWP). Infrasound has shown its ability in probing the upper atmosphere (e.g. Donn and Rind, 1971; Le Pichon et al, 2009). A key benefit of infrasound is the sensitivity to both temperature and wind in a region where atmospheric observations are scarce. Beyond the lower stratosphere, wind information is even missing completely (**??** Chapter Lee et al). SSWs are a good starting point to apply novel techniques based on infrasonic analysis. Therefore, studying SSWs using infrasound is part of the roadmap on the use of infrasound data for weather and climate monitoring of the Atmospheric Dynamics Research Infrastructure in Europe - ARISE - project. This chapter describes how infrasound can provide additional insight in SSW events and how this information can be used in current atmospheric models for, example given, stratospheric predictability evaluation. First we elucidate the relation between infrasound and sudden stratospheric warmings and why studying these events is important for both weather and climate as well as for infrasound montoring. Secondly, an overview of infrasound studies of SSWs are listed, evolving from observations to a comprehensive approach to explore the middle atmosphere. Finally, an outlook is given of this first step of infrasound on the path towards data assimilation.

2 Sudden stratospheric warmings

SSWs are regularly occurring features in winter on the northern hemisphere (Charlton and Polvani, 2007) characterised by dramatic changes in the stratospheric wind and temperature. Sudden stratospheric warmings (SSWs) are the strongest manifestation of the stratosphere-troposphere interaction (Charlton and Polvani, 2007; Shaw and Shepherd, 2008; Gerber et al, 2009).

2.1 Principle mechanism

In the stratosphere, the temperature increases with height to a maximum at the stratopause due to the absorption of solar ultraviolet radiation by ozone (Holton, 2004). This unequal solar insolation induces a temperature gradient from summer pole to winter pole, driving the circumpolar vortex. For this induced geostrophic circulation, the Coriolis force balances the acceleration due to moment flux convergence to maintain the thermal-wind balance (Muench, 1965). The seasonal variation

in the atmosphere's heat balance changes the direction of the polar vortex, typically around the vernal and autumnal equinoxes. In summer, during polar day, the circumpolar vortex is easterly, characterised by a stable stratospheric wind and temperature structure. In winter, the westerly circumpolar vortex is stronger but unstable as vorticity is not conserved.

During polar night, the high-latitude westerly jets provide a waveguide for vertical propagation of quasi stationary planetary waves, primarily of zonal wave numbers 1 and 2 (Holton, 2004). Rossby waves propagate from the troposphere up into the stratospheric polar vortex (Matsuno, 1971; Holton, 2004). When the winter stratospheric polar vortex is triggered by the planetary scale disturbances, eddy potential vorticity flux is deposited in the stratosphere. This Rossby wave breaking decelerates the zonal mean flow, reducing the pole-to-equator mean temperature gradient (Charney and Drazin, 1961). As the wind zonal mean flow is to remain geostrophic, the stratospheric polar temperature increases. Due to the repeated Rossby wave breaking the stratospheric polar vortex gets highly distorted, breaking the polar vortex. When these stratospheric changes are severe, it is known as a sudden stratospheric warming. Two types of SSW occur, a vortex displacement away from the pole and a vortex split into two daughter vortices (Charlton and Polvani, 2007). SSWs occur mainly on the northern hemisphere since the enhanced upward propagation of Rossby waves is primarily induced by continental blocking (Kodera et al, 2013).

Sudden stratospheric warmings can be classified in four characteristic scales, however, various definitions exist for each. The definition according to the World Meteorological Organisation (WMO) and Labitzke (1977).

Major	A latitudinal mean temperature increase poleward of 60° latitude with an associated circulation reversal and breakdown of the polar vortex.
Minor	Zonal winds in the stratosphere and the meridional temperature gradient weaken but do not lead to a breakdown nor reversing of the polar vortex.
Canadian	A warming with strong non-zonal character. The net zonal winds can reverse but the polar vortex does not break down.
Final	A major warming which occurs in late winter, due to the change from polar night to polar day each spring.

2.2 Importance to weather and climate

The importance of the middle atmosphere increased notably since the evidence indicating that processes in the stratosphere couple to the troposphere (Baldwin and

Dunkerton, 2001; Limpasuvan et al, 2004; Charlton et al, 2004; Shaw and Shepherd, 2008). Progress has been made towards a more comprehensive representation of the atmosphere in order to to better capture stratospheric-tropospheric coupling (Randel et al, 2004; Charlton-Perez et al, 2013).

Significant effort has been made by NWP to better characterise SSWs. Accurate SSW prediction is justified due to its delayed impact on the weather as experienced on the Earth's surface (Sigmond et al, 2013; Tripathi et al, 2015). Recently, a significant update has been made to the numerical scheme in the stratosphere of the Integrated Forecast System (IFS) at the European Centre for Medium-range Weather Forecasts (ECMWF) (Diamantakis, 2014), leading to an improved characterisation of SSWs. Since the stratospheric region is notoriously difficult to monitor (**??** Chapter Lee et al), NWP is limited to only a few satellite based radiance observation techniques in the stratosphere. These radiance observations are dominated by Advanced Microwave Sounding Unit type A (AMSU-A), capable of capturing the fast temperature variations related to the SSW. Due to this very rapid changes, the NWP model first-guess field and assimilated observations can differ significantly at the onset of a warming. Significant discrepancies result in a possible rejection of all good AMSU-A data. Consequentially, the quality of both the stratospheric analysis and forecast is inadequate (Diamantakis, 2014; Smets et al, 2016). Further improvements in SSW predictions can be obtained from better resolving the stratosphere (Gerber et al, 2009; Roff et al, 2011) and mesosphere (Coy et al, 2011) together with assimilating data using additional techniques (**??** Chapter Lee et al).

3 Infrasound and sudden stratospheric warmings

Infrasound, used as a waveform verification techniques for the Comprehensive Nuclear-Test-Ban Treaty (CTBT), notably progressed in its ability as a remote sensing technique for the upper atmosphere (e.g. Le Pichon et al, 2010). Since the treaty opened for signing in 1996 (Dahlman et al, 2009), there has been a renaissance in the development of using ground-based infrasound arrays for upper atmospheric remote sensing (e.g. Lalande et al, 2012; Assink et al, 2013; Fricke et al, 2014; Chunchuzov et al, 2015). Latest tendencies of infrasound studies touch upon the evaluation of stratospheric specifications, i.e., analyses (Assink et al, 2014; Le Pichon et al, 2015), ensemble members (Smets et al, 2015) and forecasts (Smets et al, 2016), and the study of SSW events (e.g. Smets and Evers, 2014).

3.1 Sensitivity of infrasound to SSWs

Infrasound propagation strongly depends on the state of the atmosphere, which may result in either reflection or refraction and attenuation of the signal. The low frequency signals propagate efficiently over long distances, since attenuation is in gen-

eral relatively low. In a horizontally layered atmosphere, infrasound propagation can be approximated to first order by the effective speed of sound $c_{\text{eff}} = c_T + w_a$, a function of the adiabatic speed of sound $c_T \approx 20.05\sqrt{T}$ for temperature T and the horizontal wind in direction of propagation w_a (Godin, 2002). Refraction of the infrasonic signals is constrained by variations in the speed of sound gradient (Brekhovskikh and Godin, 1999); propagating upwards for a decrease in sound speed gradient and downwards for an increase. The refractivity or ducting of the atmosphere can be indicated by the ratio of the effective speed of sound at an altitude with respect to the effective speed of sound at the ground. Signals refract back to the ground when the effective speed of sound ratio is approximately one or larger; indicating an atmospheric waveguide or duct. Therefore, infrasound is most sensitive at the refracting or return altitude (**??** Chapter Jelle).

In general, three different atmospheric waveguides can be differentiated: signals refracting in either the troposphere, stratosphere, or thermosphere. The tropospheric waveguide is mainly bound by wind, i.e., the jet stream around the tropopause ($\sim$10 km). The stratospheric waveguide depends on the increase of both wind and temperature, induced by the temperature increase due to the presence of ozone driving the stratospheric polar vortex. Both tropospheric and stratospheric waveguides are predominantly anisotropic due to the strong wind jets. Propagation in directions opposite the tropospheric and stratospheric wind is hardly possible. The thermospheric waveguide is dominated by strong positive temperature gradient above the mesopause, causing more isotropic ducting. However, infrasound from these return altitudes is strongly attenuated (Sutherland and Bass, 2004; Assink et al, 2012). During SSWs, the top of the stratospheric waveguide may extend from the lower stratosphere to the lower mesosphere. In addition, a SSW affects the atmospheric waveguide, ranging from minor variations to dramatic changes, detectable in the infrasound observations at the ground (e.g. Donn and Rind, 1971; Evers and Siegmund, 2009; Hedlin et al, 2010; Assink et al, 2014).

3.2 Importance to infrasound monitoring

Improved knowledge and observations of stratospheric warmings is not only of great interest to Numerical Weather Prediction but as well to infrasound monitoring purposes, e.g., CTBT treaty verification. IMS infrasound network capabilities considering long range propagation aspects are determined by the state of the stratosphere. Stratospheric variability, e.g., during equinox periods and stratospheric warmings, strongly influences the detectability of infrasound (Le Pichon et al, 2008, 2010; Tailpied et al, 2017). During the last decade, the number of studies coming across odd atmospheric conditions related to SSWs has increased significantly.

On 19 February 2008 a large bolide were observed by several hundreds of broadband seismic stations in the U.S. Pacific Northwest. Hedlin et al (2010) encounter a unexpected predominant easterly propagation direction of the acoustic-to-seismic signals related to a sudden stratospheric warming event. Infrasound propagation

simulations using ECMWF/ G2S atmospheric specifications were unable to explain the observation. The study of Hedlin et al (2010) indicates for the first time discrepancies in atmospheric models by infrasound during a stratospheric warming.

In 2009 and 2011, three large-scale infrasound calibration experiments were conducted to test the International Monitoring System (IMS) infrasound network of the CTBT and provide ground truth data for infrasound propagation studies (Fee et al, 2013). For the 2011 experiments, portable infrasound arrays in the source region were deployed to the east of the of the source, aiming to take advantage of the typically winter westerly tropospheric and stratospheric winds. However, prior to the 2011 tests a minor stratospheric warming occurred (see Subsection subsec:Assink2014b), changing the stratospheric duct from westerly to easterly. Infrasound propagation and detectability were strongly influenced. The results of the Sayarim experiments, designed to test the IMS, would have been significantly different if the explosions had occurred a week earlier.

The study of De Angelis et al (2012) demonstrates an automatic infrasound and seismo-acoustic eruption detection algorithm for real-time volcano monitoring operations in remote regions. Acoustic propagation modelling shows how strong tropospheric ducting allow infrasound to travel long distances across the Aleutian Arc. For the stratospheric signals, De Angelis et al (2012) point out an unusual winter stratospheric jet characterised by easterly winds which may have been caused by a sudden stratospheric warming event.

More recently, the study of Assink et al (2016) analysed the atmospheric infrasound of the underground nuclear tests by the Democratic Peoples Republic of Korea (DPRK) of 12 February 2013 and 6 January 2016. During the 2013 and 2016 tests, the stratospheric waveguide was in a very different state. Clear detections were made in the Russian Federation (I45RU) and Japan (I30JP) in 2013 at stations from the International Monitoring System. Both tropospheric and stratospheric refractions arrived at the stations. In 2016, only one weak return was potentially observed at I45RU due to presence of an early stage SSW. Despite the stratospheric variability, the 2016 event could be simulated using the ECMWF HRES forecast. Observations and the modeled parameters associate this arrival to both the tropospheric and stratospheric propagation paths. Identification of the, rather unstable, detection is much dependent on the processing parameters and might be missed with different settings for the bin size, overlap, and corner frequencies of the band-pass filter.

Therefore, understanding the detectability of infrasound and its dependencies is crucial for successfully applying infrasound as a verification technique.

4 Overview of studies from observations to a comprehensive approach

4.1 From the 1970's to 2009

The first infrasound signature of a stratospheric warming goes back to the pioneering studies by both Donn and Rind, intrigued by the ability of natural infrasound to probe the upper atmosphere. Typical for their studies is the use of ambient noise from interacting ocean waves, microbaroms and microseisms, as a continuously natural mechanism for exploring the atmosphere. Fundamental to their studies of the SSW is the identification of a characteristic diurnal variation in the amplitude of the ambient noise observations. Donn and Rind (1971) relate amplitude changes to the state of the atmosphere, independent of any variation in the source. In winter, high amplitudes with a strong semidiurnal variation are denoted while summer amplitudes are lower with a weak diurnal variation. They associate typical amplitude variations to viscous dissipation associated with reflection height variation, described more thoroughly in Rind and Donn (1975). More important is the link between abnormal microbarom intensities in the early winter of 1967-1968 to variations in the stratosphere; the first infrasonic signature of a stratospheric warming. As the winds turn, around the equinoxes and during SSWs, the amplitudes of ambient coherent infrasound noise decreases.

The stratospheric warming of December 1967 is studied more elaborate in Donn and Rind (1972), including early propagation simulations. In addition to amplitude variations, Rind et al (1973) made use of microbarom trace velocities for estimating upper air wind speeds. The latter led to the studies of Rind and Donn (1975, 1978), utilising sound celerity variations from infrasound-seismic ambient noise variations as a preliminary atmospheric probe. These studies came to a stop when nuclear tests were diverted to the subsurface under the Limited or Partial Test Ban Treaty. Nevertheless, Donn and Rind paved the path for using natural ambient noise as a comprehensive technique for monitoring several upper atmospheric parameters.

Microbaroms are atmospheric pressure oscillations radiated from non-linear ocean surface wave interaction at double the ocean wave frequency (Gutenberg, 1939; Longuet-Higgins, 1950; Posmentier, 1967). Interacting large regions of high-energetic ocean waves of similar frequency with opposite directions, e.g., ocean swell and marine storms, radiate almost continuously acoustic energy well characterised by a radiation frequency of 0.2 ± 0.1 Hz. Microbaroms dominate the infrasound ambient noise field, making them a preferred source for passive atmospheric probing.

Microbarom source modelling can be obtained using a two-fluid model, over air and seawater, and a coupled ocean-wave model providing the sea state

(Hasselmann, 1963; Brekhovskikh et al, 1973). Air-sea coupling is crucial due to the two-way interaction of surface winds and ocean waves (Janssen, 2009). The state-of-the-art infrasound microbarom radiation source model, assuming an infinite ocean depth (Waxler and Gilbert, 2006), has been validated by Walker (2012) and Stopa et al (2012), studying ambient swell and hurricane induced microbaroms, respectively. The more recent Waxler et al (2007) microbarom radiation model takes into account the effect of resonance due to bathymetry, affecting the source location, amplitude, and frequency, and has been validated by Smets and Evers (2014).

4.2 The 2009 major SSW: an infrasonic game changer

Recently, with the signature of the Comprehensive Nuclear-Test-Ban Treaty in 1996, the use of infrasound as a passive atmospheric probe gained renewed attention. Several authors realised the potential of the IMS infrasound network in global monitoring of natural infrasound for stratospheric variations related to a stratospheric warming (e.g. Le Pichon et al, 2006; Evers and Siegmund, 2009; Le Pichon et al, 2009). However, it lasted until 2009 before a new infrasound monitoring study of a SSW appeared.

In January 2009, a major sudden stratospheric warming caused drastic changes in the stratosphere. The midwinter westerly stratospheric vortex shortly displaced and elongated, followed by a full vortex split and an increased amplitude of the zonal wavenumber number 2 planetary waves. For several days, two vortices and reversed winds specify the stratosphere (see Figure 1 and Subsection 4.5). By the beginning of February 2009 the stratosphere recovers to its typical midwinter state.

The infrasonic signature of the 2009 SSW is described by Evers and Siegmund (2009), exploiting back azimuths of oceanic noise at the IMS infrasound arrays in the northern hemisphere. For the first time, passive infrasonic observations at the surface provided detailed information on upper atmospheric processes on a global scale. IMS arrays north of 15°N detect a large amount of coherent ambient infrasound noise, as long as the local wind speeds are low. Sensitivity of infrasound arrays to sources located in specific directions is controlled by the atmospheric state, described in Subsection 3.1. Therefore, variations in the direction and intensity of the stratospheric polar vortex, such as during a SSW, seriously affects the microbaroms detectability in terms of back azimuth. Figure 1 illustrates the stratospheric wind and temperature at 50 km prior to the SSW and during the vortex split. The SSW caused ambient noise observations to arrive from the opposite direction than expected during regular midwinter conditions at multiple infrasound arrays, marked in Figure 1. In normal winter conditions, westerly ambient noise observations are expected, since the stratospheric ducts is favourable to down wind conditions. However, throughout the major stratospheric warming the polar vortex breaks down and

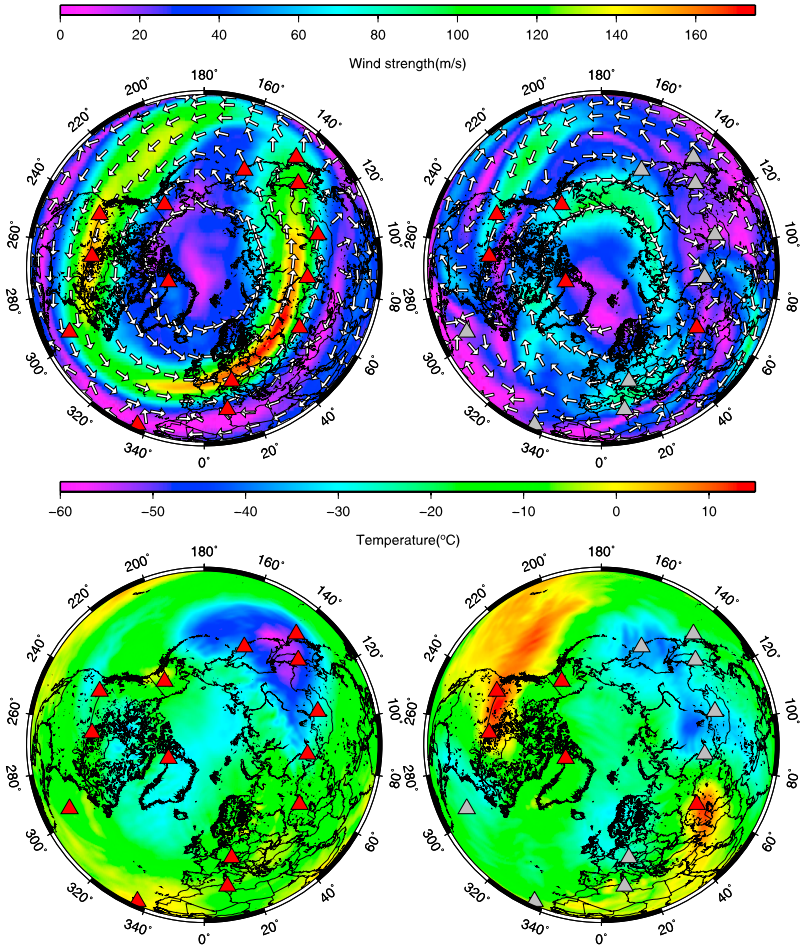

Fig. 1 From Evers and Siegmund (2009). (top) wind and (bottom) temperature at 50 km altitude from ECMWF analyses. (left) Valid for 2009, January 2 at 00 UTC, prior to the SSW; (right) values during the vortex split phase of the SSW on January 23 at 00 UTC. The red triangles in the right column indicate arrays which sensed the SSW, the grey triangles represent arrays where no clear signature was found in the observed back azimuths.

reverses which alters the duct from westerly to easterly. This dramatic change is clearly denotable in microbarom observations by an altered or (dis)appeared microbarom source region, leading up to the infrasonic signature of a SSW. Evers and Siegmund (2009) indicate clear infrasonic signatures of the stratospheric warming observed in Greenland (IS18), Alaska (IS53), over the western US (IS56) and central Canada (IS10). Even in Kazakhstan (IS31) slight changes in the retrieved back azimuths are notable. At the Russian arrays (IS44, IS45 and IS46) no pronounced changes in the observed back azimuths are visible. Similar results are also found for the German (IS26), Japanese (IS30), Mongolian (IS34) and Tunesian (IS48) arrays.

4.3 Anomalous infrasound propagation in a hot stratosphere

So far, less attention has been paid to stratospheric temperature variations, next to the wind. Evers et al (2012) studied the temperature effect in the stratosphere on infrasound propagation. A case study of an explosion indicates a significant reduction of the size of the classical stratospheric shadow zone. During the January 2010 SSW, the extent of the classical stratospheric shadow zone (~ 200 km) reduces by a factor of 2, leading to extremely small shadow zones. When the temperature gradient in the vicinity of the stratopause is higher than the Earth's surface temperature, for example, throughout a SSW, pure temperature gradient induced refractions can occur.

The occurrence of such conditions is quantified by analysing ten years ECMWF analyses, four times per day. The stratospheric shadow zone is simulated by ray theory in a 1-D model in direction of the wind at 50 km. A minimum value in stratospheric shadow is obtained by using the steepest gradient in c_{eff}. Stratospheric returns occurred 62% of the time and mostly in winter (51%). Hardly any returns are observed around the equinoxes due to the lack of significant downwind component at 50 km altitude. Very small shadow zones of less than 100 km occurred 3% of the time. For 1% of the time no additional downwind component w_a is necessary to enable refraction back to the Earths surface, mostly associated with SSWs.

The existence of small shadow zones is confirmed by infrasound from mining blasts in southwestern Siberia, Russia, observed by IMS infrasound array IS46 (Russia). Events are obtained from the Reviewed Event Bulletin (REB) from the International Data Center (IDC) for verification of the CTBT. Locations are seismically determined using IMS seismic arrays in Russia using at least two seismic arrays. Locations errors are in the order of a couple of kilometers. Selected events in this low-seismic area, within the back azimuthal interval between 59.5° to 90.5° of IS46 at a maximum distance of 250 km, most likely correspond to open pit mining. Stratospheric conditions of wind and temperature correspond to the number of detections at I46RU, see Figure 2, and consequently to the variation in the apparent velocity c_{app} of the events. c_{app} is the horizontal projection of the propagation velocity vector. For a layered medium, apparent velocity is invariant (Pierce, 1981). The infrasound signals correspond to stratospheric refractions, indicated by the agreement of the structure of c_{app} to the structure of the stratosphere. This would not have been the case for tropospheric arrivals. During the equinoxes hardly any detections are made and during winter conditions, summer-like apparent velocities appear which could only be caused by SSWs. However, it should be noted that more stratospheric arrivals are observed than predicted by the modelling. Fine-scale structure in the wind and temperature caused by internal gravity waves, not resolved by, e.g., the ECMWF models, is responsible for generating additional arrivals (Kulichkov et al, 2010; Revelle, 2010; Chunchuzov et al, 2011).

Some observed c_{app} lay below the c_T curve, which is physically impossible (see Figure 2, fourth panel). The adiabatic speed of sound c_T is the lowest possible propagation velocity. Lower values of c_{app} are in first order attributed to uncertainties in array processing (timing and c_{app}) and the surface temperature, which

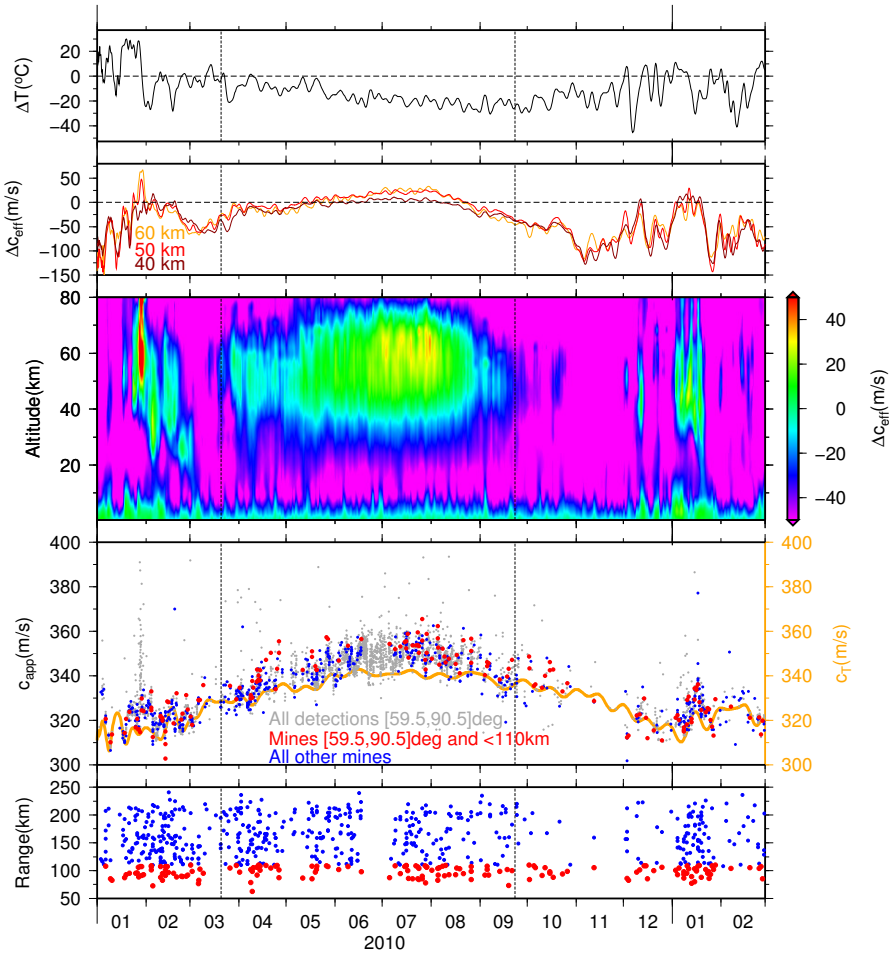

Fig. 2 From Evers et al (2012). From top to bottom are listed; atmospheric specifications and REB detections at IMS infrasound array IS46 (Russia) from seismic ground-truth locations. Only associated infrasound detections within the back azimuthal interval between 59.5° to 90.5° are used. Vertical dashed lines indicate the vernal and autumnal equinox. (first panel) The temperature difference between 50 km altitude and the surface, ΔT. The c_T, Δc_T and ΔT curves are smoothed with a polynomial fit. (second panel) Cross sections from Δc_{eff} at an altitude of 40, 50 and 60 km. (third panel) The difference between the effective sound speed at a certain altitude and near the surface, colour coded as Δc_{eff}. The latter are derived from ECMWF analyses at 54.0°N, 85.5°E. (fourth panel) The apparent sound speed, c_{app}, of the detections. The red and blue dots are seismic locations from the REB assumed to correlate with mining activity, i.e., blasting. Mines at a distance of less than 110 km are denoted by red dots, all other detections within the back azimuth range are added as grey dots. The surface sound speed c_T is given as orange line and calculated from the temperature. (fifth panel) The distances of the mining activity sources with respect to IS46 as function of time.

forms the basis for c_T. The temperature is obtained from NWP specifications and is not an actual measurement at the station. Nevertheless, the general trend of stratospheric variations, i.e., summer versus winter characteristics, turning winds around the equinoxes and SSWs, are reflected in the observed c_{app}. Lower surface temperatures and stronger gradients in c_{eff} during winter explain the lower values of c_{app} with respect to summer.

Observations at IS46 deliver the proof for the existence of extremely small shadow zones, less than 100 km in size, for stratospheric arrivals. These results are applicable to a broad latitudinal range defined as the stratospheric surf zone, i.e., 20°N to 60°N where a rather stationary flow of stratospheric air occurs.

4.4 Bidirect infrasonic ducts associated with a minor SSW

Donn and Rind (1972, Subsection 4.1) and Evers and Siegmund (2009, Subsection 4.2) reported on significant azimuthal reversal due to the reversal of the zonal jet as a result of a major warming event. Nevertheless, Assink et al (2014) denoted simultaneous arrivals from two nearly opposite stratospheric ducts during a minor warming. In January 2011, a bidirectional stratospheric duct persisted for two weeks In the wake of a minor SSW. This situation occurred just prior to the 2011 Sayarim experiments (Fee et al, 2013), which took place on 24 and 26 January 2011 (see Subsection 3.2). The existence of bidirectional ducting during stratospheric warming events has not been considered in the past.

The development of a bidirectional duct has significant effects on infrasound propagation in the middle atmosphere, which is typically expected to be unidirectional. Such ducting significantly improves infrasound detection capability during these periods, since the anisotropy is strongly reduced. In general, the detectability

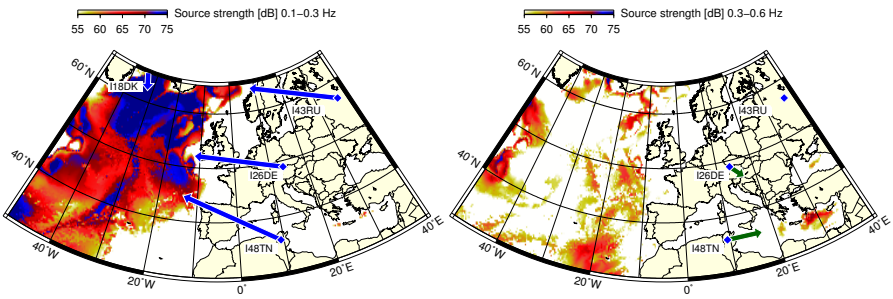

Fig. 3 Microbarom source region predictions for two distinct frequency bands, computed using the source model described by Waxler et al (2007) and ECMWF HRES-WAM two dimensional ocean wave spectra, for 17 January 2011 00 UTC. The computations for the (a) 0.1–0.3 Hz and (b) 0.3–0.6 Hz frequency bands are shown, respectively. Blue and green arrows correspond to observed back azimuth directions at IMS infrasound arrays IS26 (Germany), IS37 (Norway), and IS42 (Tunesia), for the specific frequency ranges.

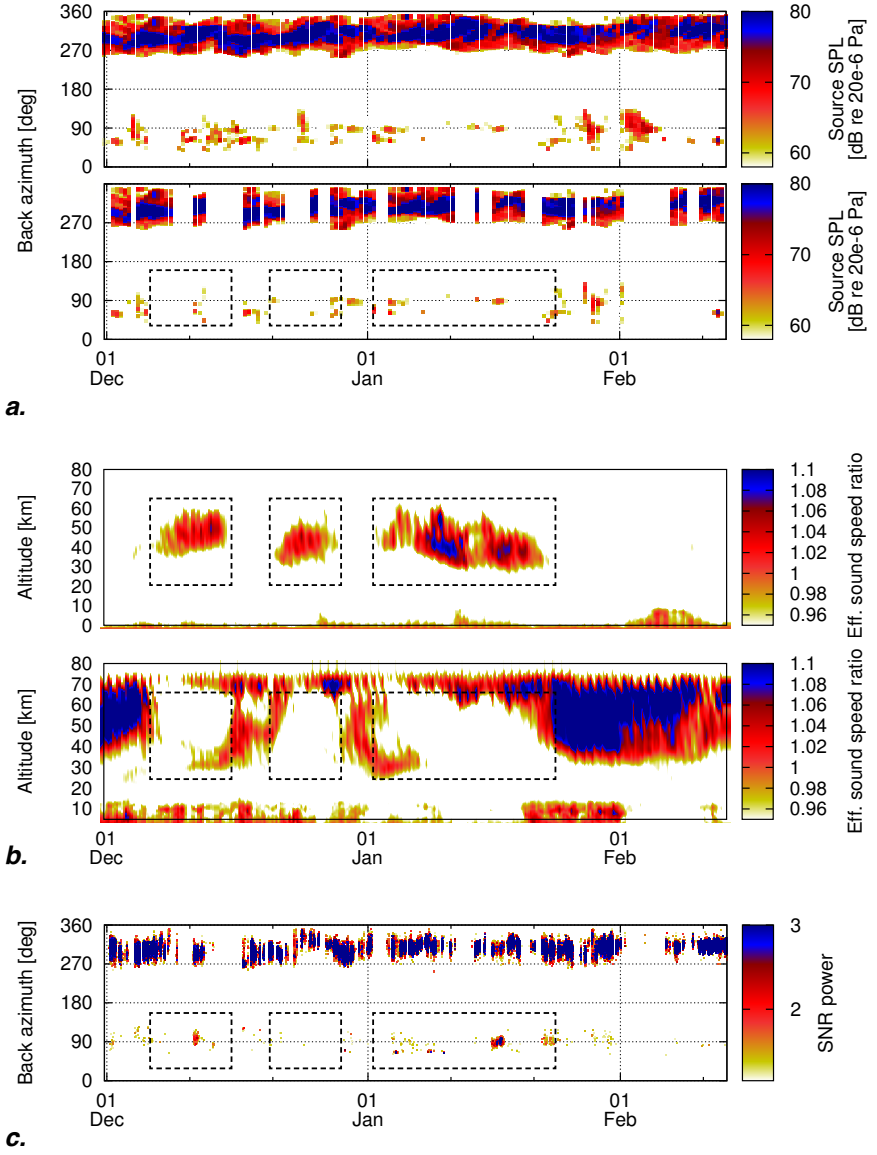

Fig. 4 Figure from Assink et al (2014). (a) Microbarom source activity in the Atlantic and Mediterranean Basins, modeled using ECMWF HRES-WAM two dimensional wave spectra and the Waxler and Gilbert (2006) source model. The back azimuths with respect to IS48 (Tunesia) and the source intensity is given as a function of time. While a continuous, broadband of energetic microbarom sources are present in the northwest, the Mediterranean activity is more sporadic. The top frame shows all sources, the bottom frame shows the source activity for when local winds are less than $1\,\mathrm{m\,s^{-1}}$, leading to low wind noise conditions and increased infrasound detectability. Thus, the remaining microbarom sources are effective sources. (b) Effective sound speed ratio values as a function of altitude and time for (top) westward and (bottom) eastward propagation. (c) Infrasound detections during the winter of 2010–2011. Intervals of bidirectional ducting conditions are indicated with dashed rectangles; the eastward duct nearly always exists. During favourable conditions, microbarom signals from two opposite directions are detected at IS48.

is determined by the source strength, distance to the source, atmospheric wind and temperature, and the ambient noise conditions near the receiving array (Evers and Siegmund, 2009).

The existence of the bidirectional duct has been demonstrated at IMS infrasound array IS48 (Tunesia). The bidirectional ducting effect is clearly captured at IS48, due to its favourable location with respect to microbarom sources at both sides of the station. Two microbarom signals, from nearly opposite back azimuth directions are observed in January 2011. A strong and persistent signal from the northwest, with frequencies around 0.2 Hz, is detected with a weaker signal from the east, in the 0.2–0.6 Hz band. The observed microbaroms sources, induced by non-linear ocean surface wave interaction, are explained by source modelling (Waxler and Gilbert, 2006) based on two dimensional ocean wave spectra from the ECMWF operational analysis HRES-WAM (High RESolution WAve Model) coupled deterministic ocean-atmosphere model. Source modelling, see Figure 3, reveals a previously unidentified microbarom source region in the eastern Mediterranean besides the more typical microbarom source region in the Atlantic Ocean. Figure 4a shows microbarom source activity in the northern Atlantic and eastern Mediterranean Basins in terms of back azimuth with respect to IS48 as a function of time. The detectability is mostly constrained by the local noise conditions, assuming efficient propagation conditions and a relatively nearby microbarom source. Low wind noise conditions are defined as local winds less than $1\,\mathrm{m\,s^{-1}}$, similar to Le Pichon et al (2005), shown in Figure 4a (bottom frame). Figure 4b shows the ducting conditions throughout the winter of 2010–2011 in direction of the northern Atlantic and Mediterranean in terms of effective sound speed ratio as a function of altitude. Several intervals of bidirectional ducting conditions exist throughout the winter of 2010–2011, indicated in Figure 4 by the dashed rectangles. The most significant interval occurs during January 2011. Note that the eastward duct would have disappeared if a major SSW had occurred. While a continuous, broadband of energetic microbarom sources is present in the northern Atlantic Basin, the eastern Mediterranean activity is more sporadic and weaker.

The observed directions (Figure 4c) correspond well with the predicted source locations for low wind noise conditions (Figure 4a, bottom frame) . While the frequency bands of the two source directions overlap, the Mediterranean signal is coherent up to about 0.6 Hz. This observation is consistent with the predicted sources. Microbarom source predictions indicate various high-intensity sources regions are present in the Atlantic Ocean in the classic microbarom band 0.1–0.3 Hz. At higher frequencies, the Atlantic source regions weaken and source regions appear in the eastern Mediterranean Sea, in between Crete and Cyprus. As the Mediterranean signal is typically much weaker than the Atlantic signal, such events are predominantly detected when beam forming specifically toward the east.

Signals from both directions are detected when all criteria are fulfilled; during intervals of bidirectional ducting with low local noise conditions and when microbarom sources are sufficiently strong. Around 10 December and 17 January 2011 the most significant eastward detections occur, indicated by the first and third dashed rectangle in Figure 4, respectively. These detections correspond with the onset and

offset of bidirectional ducting conditions throughout December 2010 to February 2011. Only very few detections from the east are made during the second anomalous period in December 2010, likely due to the presence of strong local winds that masked the microbarom sources in the eastern Mediterranean (see Figure 4a). Around 17 January, the signal intensity of both signals is about equal.

4.5 Life cycle of a major SSW

Evers and Siegmund (2009, see Subsection 4.2) obtained the infrasonic signature of a sudden stratospheric warming from the dramatic changes in the back azimuth of the observed ambient noise. The 2009 major SSW is re exploited to better understand the relation between the variations of the stratospheric polar vortex and the altered microbarom observations. Smets and Evers (2014) incorporate additional signal characteristics to acquire more insight complete view on the variations in stratospheric wind and temperature. In addition, microbarom source modelling and infrasound propagation modelling is applied to provide insight in the sensitivity of the infrasonic signature.

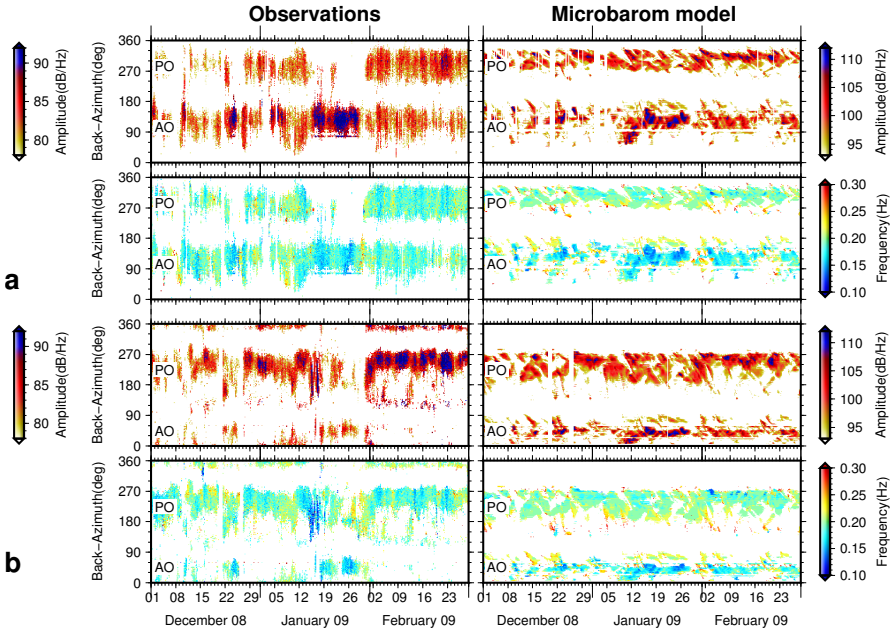

Fig. 5 Figure from Smets and Evers (2014). Comparison of the microbarom observations (left) and simulations (right), for (a) IS18 and (b) IS53. Each subfigure shows (top) the peak spectral amplitude with (bottom) the corresponding frequency, for windows of one degree in back azimuth and one hour for the observations and six hours for the modelled microbaroms. Gaps in the observations, due to high wind noise or data loss, are recreated in the microbarom predictions.

The study of Smets and Evers (2014) focusses on the northerly IMS infrasound arrays IS18 (Greenland) and IS53 (Alaska), since these arrays have the most pronounced and detailed signature (Evers and Siegmund, 2009). Figure 5 (left) shows the observed microbarom amplitudes and frequencies as a function of back azimuth over time. Note the infrasonic signature during the second half of January 2009. Ambient noise observations at IS53 alter from the Pacific Ocean (PO) to the Atlantic Ocean (AO) while the PO microbaroms disappear at IS18 during the SSW. Microbaroms are highly dynamic and dependent on the atmosphere, surface winds and ocean waves exchange momentum in both ways (Janssen, 2009). In order to understand the signature of the varying stratospheric vortex in the ambient noise observations, the source variation is isolated by simulating the microbarom sources. Spectral microbarom amplitudes are simulated using the theory of Waxler et al (2007), including bathymetry resonance effects, and two dimensional ocean wave spectra provided by the ECMWF HRES-WAM coupled ocean-wave model. Microbarom simulations for the AO and PO are shown in Figure 5 (right) projected to the point of view of infrasound arrays IS18 and IS53. Figure 5 shows a good first order agreement between the observations and microbarom predictions in the absence of propagation effects. Microbaroms are continuously active, but varying in amplitude, frequency and location over time. Good resemblance between observations and source simulations indicates the dominance of the source effect. However, clear propagation effects can be denoted, for example, the SSW signature and the northerly observations at IS18. Note that both observations and simulations indicate different frequencies for the AO and the PO due the distinctive ocean depth.

To fully understand the microbarom observations and the signature of the warming, one should know the atmospheric duct between source and receiver. IS18 simultaneously observes Atlantic and Pacific microbaroms, except during the major SSW. These simultaneous arrivals do not correspond to bidirectional stratospheric ducting, as explained by Assink et al (2014, see Subsection 4.4), as this phenomena only occurs during a minor SSW. The observations imply a stratospheric duct to the Pacific and a thermospheric duct in direction of the Atlantic during regular midwinter conditions. In midwinter, the stratospheric jet is westerly, yielding a stratospheric duct from the Pacific. Since IS18 is relatively close to the AO, approximately 2000 km, thermospheric ducting is feasible. Infrasound is most sensitive to the atmosphere at the return height. Stratospheric returns are distinguished from thermospheric returns by a characteristic (semi)diurnal signature in the observed microbarom amplitudes, without any a priori atmospheric information. The method is based on previous studies of Donn and Rind (1971); Rind et al (1973); Rind and Donn (1975, 1978), where they characterise variations of stacked microbarom amplitudes per time of day. The preliminary method involves long-period averaging, using several months of data, loosing all small scale fluctuations of interest. Other studies have identified the typical signature in various detection characteristics, e.g., the number of detections, back azimuth angle, apparent velocity, bandwidth, amplitude, and travel time(Le Pichon et al, 2005; Whitaker and Mutschlecner, 2008; Green et al, 2012; Assink et al, 2012). However, these studies make use of strong impulsive sources with a well known position, e.g., volcanoes, which makes it hard

to implement the used methodologies on varying ambient noise. In Figure 6, spectral amplitude time of day, $\bar{A}_{tod}$, for half hour windows are shown in direction of the AO and PO. Throughout the boreal winter, IS18 in AO direction shows a semidiurnal amplitude variation while the PO amplitudes indicate more of a diurnal pattern. For IS53, a clear diurnal pattern is present. However, the diurnal peak varies over time due to the movement of the source, yielding the stratospheric peak at various longitudes (and thus times).

These findings are verified by simulations, using 3-D reverse ray tracing cast in spherical coordinates and the microbarom source model, with the known implications of a vertically limited atmospheric model up to the mesosphere. Although these limitations, clear regions of stratospheric propagation can be identified, confirming the amplitude variations method. Thermospheric signals of IS18 toward Atlantic Ocean, with distance of 2000 up to 3500 km (February 2009), can be observed.

Distinguishing stratospheric from thermospheric returns. The stratosphere and thermosphere are exposed differently to solar tidal fluctuations of temperature and wind (Sutherland and Bass, 2004). This yields a different signature in the recordings at the surface, which can be used to differentiate the type of atmospheric duct.

Stratospheric returns are characterised by a weak diurnal variation. Water vapour heating in the troposphere primarily excites a diurnal thermotidal oscillation. This remains true until the thermosphere, where viscosity, conductivity, and electromagnetic damping may attenuate incoming waves (Lindzen and Chapman, 1969).

Thermospheric returns show a strong semidiurnal variation. The high attenuating nature of the thermosphere, due to the low density, causes a strong excitation to the heat generated by the absorption of solar ultraviolet radiation by oxygen around 120 km altitudes, twice a day. This semidiurnal irregular heating results in a variation of the thermospheric return height, due to a severe change in wind strength and attenuation.

The amplitude signature combined with the variation in back azimuth is used to reanalyse the 2009 SSW in detail. The effect of the warming is most pronounced for IS53 as AO microbaroms, see Figure 6(d), are only expected in summer, or, in case of a SSW. Hemispheric 10 hPa ($\sim$ 31 km) wind from the ECMWF HRES analysis in Figure 7 show the evolution of the stratospheric polar vortex before, during, and after the SSW. This indicates a displaced westerly elongated vortex from 18 tot 22 January 2009 and a vortex split from 24 to 28 January 2009, corresponding with two stratospheric vortices, followed by a recovery of until 4 Februari 2009. ECMWF analysis indicates first signatures of the warming around 22 December 2008 and 7-8 January 2009. However, infrasound observations reveal more and earlier abrupt changes, increasing in intensity and duration. These preliminary

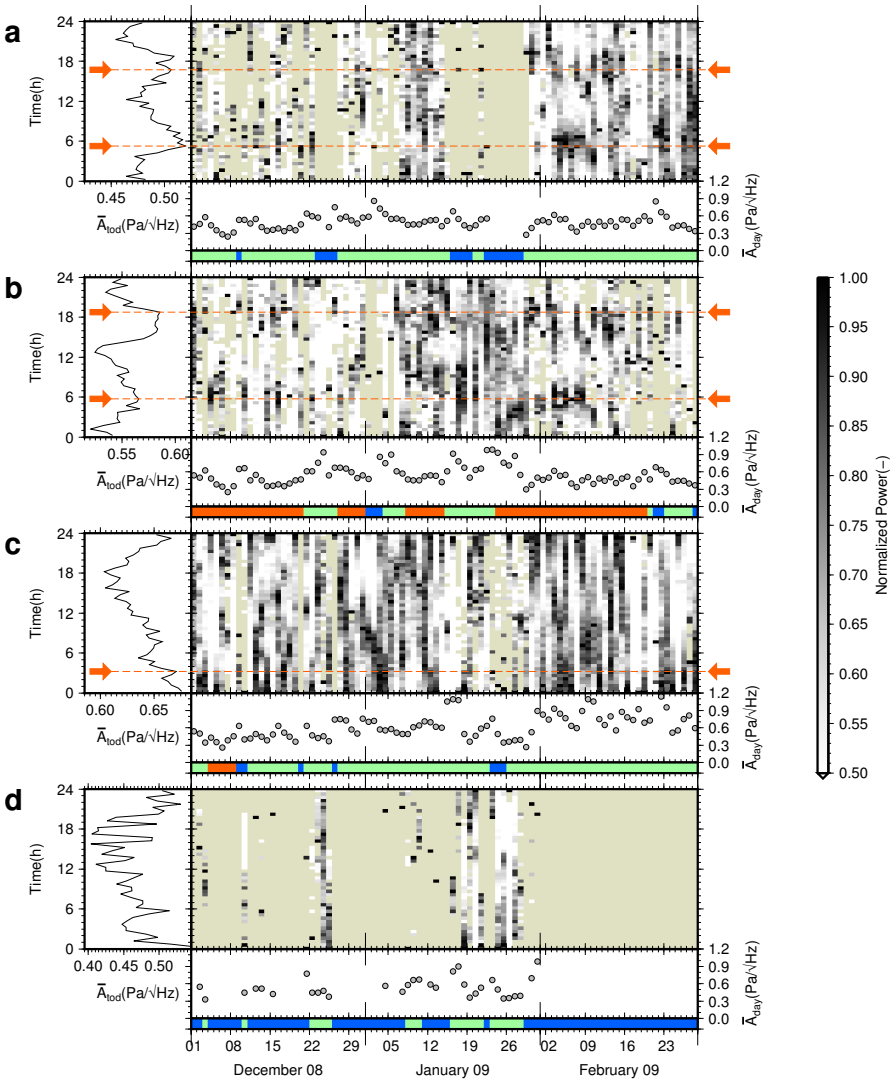

Fig. 6 Directional time averaged spectral amplitude variations (Smets and Evers, 2014). From top to bottom are shown, IS18 in direction of the Pacific Ocean (a) and Atlantic Ocean (b), IS53 in direction of the Pacific Ocean (c) and Atlantic Ocean (d), respectively. Each subfigure consists of a vertical graph (left) and an image (right) with below one horizontal graph and one colour coded bar. The vertical graph (left) shows the spectral amplitude averaged per time of day, $\bar{A}_{tod}$, for each half hour. The red arrows and dashed lines indicate the tidal peaks in the mean time of day amplitude, if present. The image (right) shows the half hour averaged spectral power, normalised per day. Each pixel column corresponds with one single day, while each row indicates the time of day. The horizontal graph shows the daily mean spectral amplitude $\bar{A}_{day}$. The colour coded bar roughly indicates manually picked periods with either no peak (blue), one peak (green) or two peaks (red) per day, respectively. Only detections are used with $SNR \geq 1.5$ for IS18 and $SNR \geq 1.3$ for IS53.

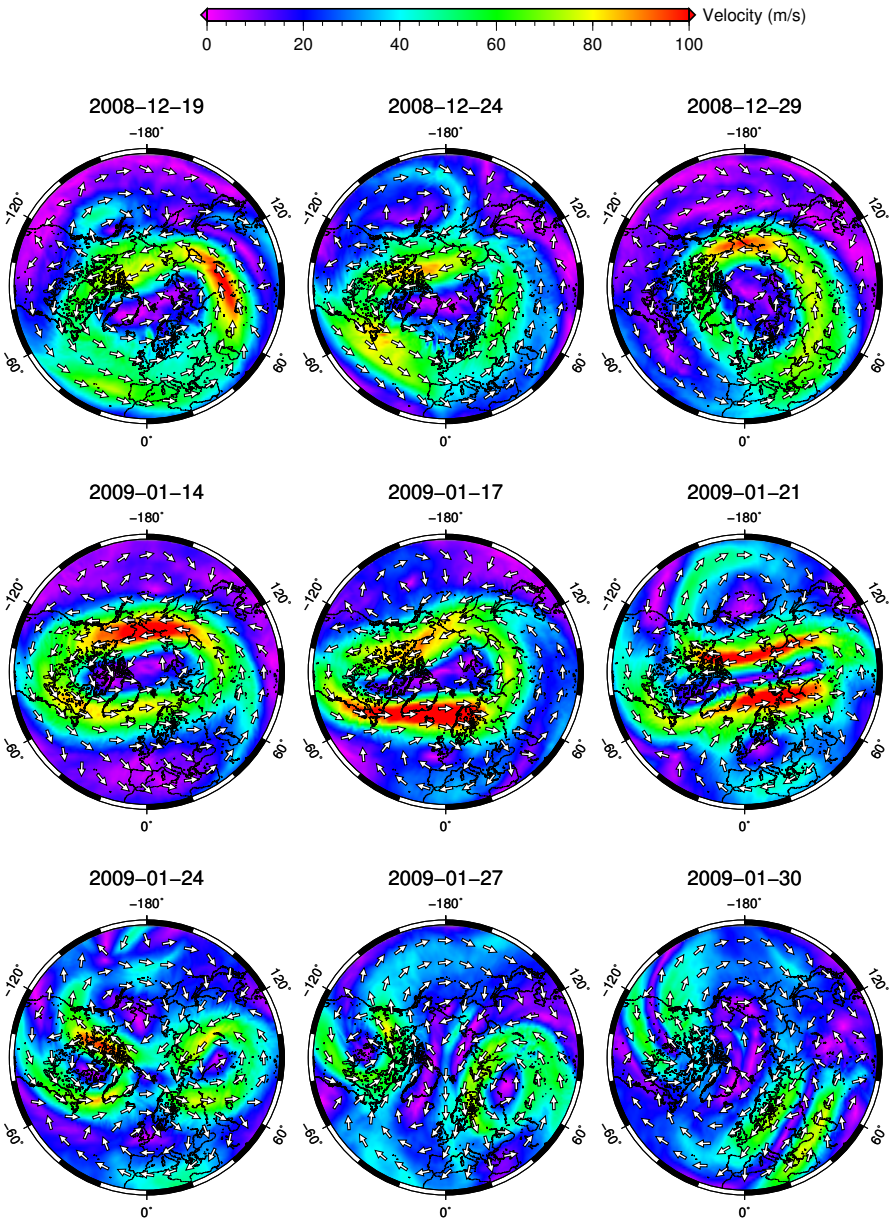

Fig. 7 From Smets and Evers (2014). ECMWF HRES analyses for wind velocity and direction at 10 hPa (∼31km) at midnight. Note the different signature of the vortex in the lower stratosphere in comparison to Figure 1, showing the wind and temperature in the upper stratosphere.

signatures correspond to Rossby wave breaking in the stratospheric polar vortex, disturbing the circumpolar vortex via momentum dumping. Rossby waves, type 2 planetary, have a typical period of 10 to 16 days, repeatedly disturbing the polar vortex (Holton, 2004). A similar pattern can be denoted in Figure 6, initiating on 3 and 10 December 2010. At the beginning of the winter, the cyclonic circumpolar vortex is strong but highly unstable, being very sensitive to any disturbance. The vortex weakens, resulting a clear AO stratospheric duct denoted at IS53, from 22 to 25 December, with diurnal peak at approximately 16 hours. A stronger longer lasting disturbance occurs from 17 to 21 January 2009, yielding a displaced and elongated rather unstable cyclonic vortex. For that period, IS53 indicates a stratospheric duct in AO direction with a diurnal maximum at approximately 14 hours. Between 23 to 28 January 2009, the cyclonic vortex becomes critically disturbed and splits into two anticyclonic vortices located above Canada and Russia. Due to these locations, no clear difference in back azimuth is present. However, the change in observed amplitude and phase shift of the (semi)diurnal signature do indicate a stratospheric variation. The anticyclonic vortices dissolve at the end of January 2009 wheres the stratosphere recovers to its normal winter situation. Because of the weak polar vortex, recovering slowly due to the gradually radiative cooling of the polar cap (Limpasuvan et al, 2005), a stable continuous stratospheric duct in PO direction is present, clearly noticeable in the microbarom observations.

The study of Smets and Evers (2014) shows the ability of observed microbarom amplitudes to provide more details on the life cycle of a SSW. Two most important differences between the infrasound observations and the ECMWF analysis are: 1) A strong AO stratospheric duct is observed from 22 to 25 December 2008 at IS53, likely corresponding to a preliminary vortex disturbances, but missing in the analysis. 2) Observations indicate an earlier recovery of the stratospheric vortex, at 30 January 2009.

4.6 SSW forecast predictability evaluation

In the study of Smets et al (2016), a novel method for the evaluation of middle atmospheric weather forecasts is introduced. For the first time, weather forecasts for different forecast steps are evaluated using infrasound. A year of near-continuous infrasound detections from Mount Tolbachik are used, observed by IMS infrasound array IS44 on the Kamchatka peninsula in Russian Federation (55.8°N, 160.3°E). Volcanoes represent valuable sources for passive acoustic remote sensing of the atmosphere, as the source location is fixed and the source is relatively well understood (Fee et al, 2010; Matoza et al, 2011; Marchetti et al, 2013).

IS44 is located at approximately 347 km south-west of Mount Tolbachik, with a true bearing of 28.11° clockwise from north. Typically, IS44 is reached after one stratospheric bounce in summer. Throughout the course of a stratospheric warming, the hot stratosphere induces shallower and shorter stratospheric bounces, making two returns possible. This effect of a hot stratosphere on the propagation of infra-

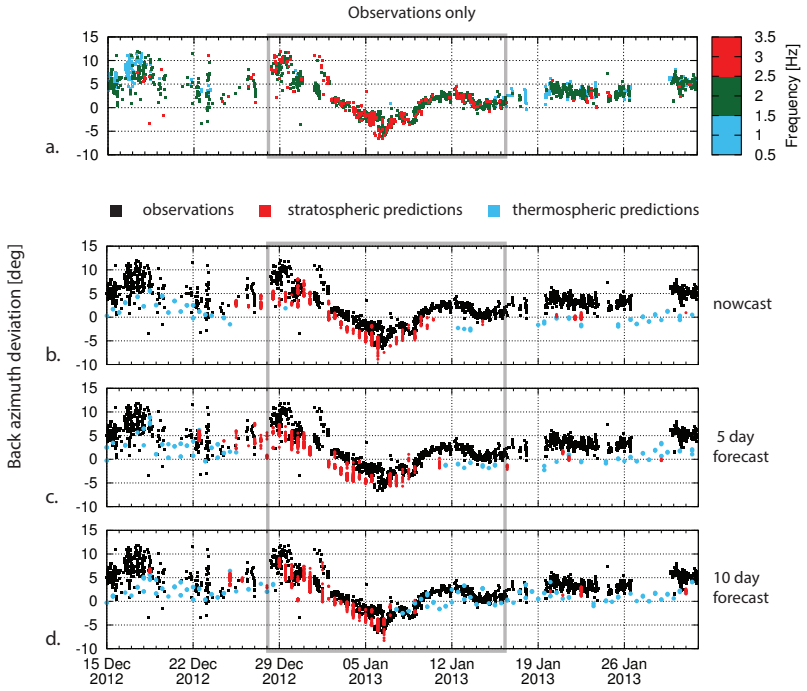

Fig. 8 Figure from Smets et al (2016). (a) Back azimuth deviation values from Mount Tolbachik infrasound detections, for which trace velocity values are shown in Figure 9a. (b–d) Comparisons between observations (black dots) and 3-D ray tracing results (red dots) as a function of time, using three different ECMWF HRES forecasts: (Figure 8b) nowcast, (Figure 8c) 5 day forecast, and (Figure 8d) 10 day forecast. The blue dots correspond to simulated arrivals that have propagated through the mesosphere and lower thermosphere, for which the MSIS and HWM climatologies have been used. The grey rectangle points to the continuous high-frequency infrasound observations interpreted as low stratospheric altitude returns (<40 km return altitude). These low stratospheric returns with sudden reversal in back azimuth are interpreted to be due to the SSW.

sound in explained by Evers and Siegmund (2009, see Subsection 4.2). The relative small acoustic wavelength and near-continuous character of the source leads to high temporal resolution sensitive to small atmospheric changes. The results in clear variations in array characteristics, such as, back-azimuth and apparent velocity (also named trace velocity), shown in Figures 8a and 9a, respectively. Figures 8a shows the back azimuth deviation, which is the difference between the true bearing and the propagation azimuth needed to arrive at the receiver location. Back azimuth deviation is a good indicator of cross-winds (**??** Chapter Jelle). The latitudinal propagation prompt an increased sensitivity to changes in the zonal stratospheric wind, dominating the cross-wind conditions. A clear infrasonic signature is denotable, marked by the grey rectangle, inducing summer-like conditions since in winter no stratospheric returns are expected. The continuous high-frequency infrasound observations are interpreted as low stratospheric altitude returns (<40 km return alti-

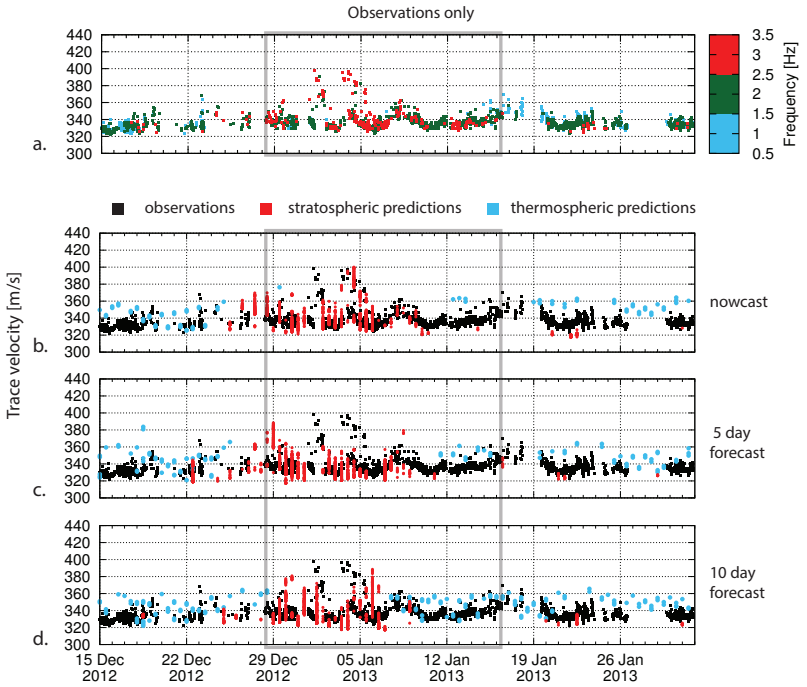

Fig. 9 Figure from Smets et al (2016). (a) Trace velocity values from Mount Tolbachik infrasound detections. (b–d) Comparisons between observations (black dots) and 3-D ray tracing results (red dots) as a function of time, using three different ECMWF HRES forecasts: (Figure 9b) nowcast, (Figure 9c) 5 day forecast, and (Figure 9d) 10 day forecast. The blue dots correspond to simulated arrivals that have propagated through the mesosphere and lower thermosphere, for which the MSIS and HWM climatologies have been used.

tude). The increase in trace velocity indicates a stratospheric temperature increase and decreased return height. A strong variation in back azimuth deviation is present, which indicates altering cross winds from easterly (positive back azimuth deviation) to westerly (negative back azimuth deviation). Therefore, these low stratospheric returns are interpreted to be due to the SSW indicating the assumed warming onset (28 December 2012) and recovery (16 January 2013).

The method of Smets et al (2016) to evaluate the stratospheric predictability, especially of interest during the SSW, is based on forward modelling the propagation of infrasound from Mount Tolbachik towards IS44. A year of near-continuous infrasound from the volcano Mount Tolbachik is compared with simulations using the high-resolution deterministic forecasts of ECMWF. An in-house developed ray tracing algorithm (cast in spherical coordinates) is used that takes into account the full effect of the 3-D inhomogeneous wind and temperature fields, see, for example, Brekhovskikh and Godin (1999). As such, array characteristics of back azimuth, trace velocity and travel time are simulated for the entire period, every 12 hours, using various forecast steps. These wavefront simulations are compared to the array

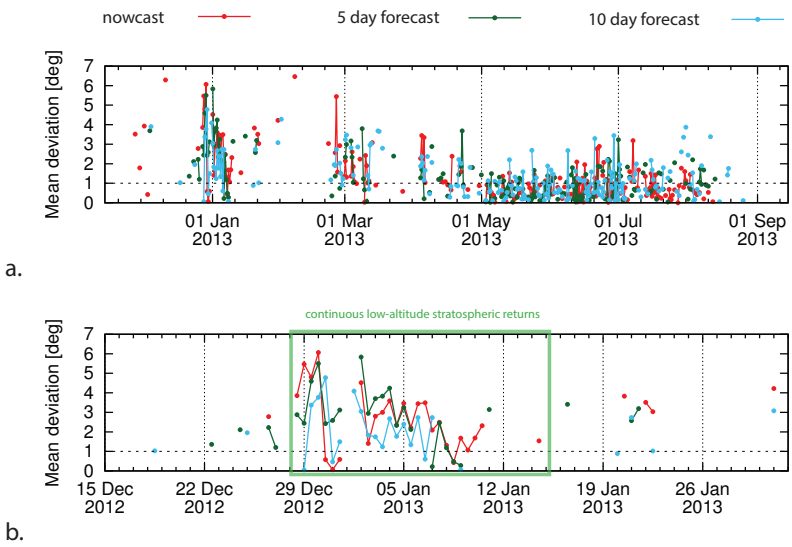

Fig. 10 (a) Estimated difference between the observed and predicted back azimuth of all returns over the full timespan of observation. Observations are averaged for 12 hour time bins and contain at least 6 detections. The different colours correspond to the different ECMWF forecasts that are used in the simulations. The lines connecting the dots indicate the continuity of the predictions. The horizontal dashed black line is indicative of the uncertainty of the infrasound array. (b) Similar as (a), but focusing on the midwinter with the SSW period (green rectangle).

observations for each forecast step. Significant inconsistencies or lack of simulated returns indicates a possible difference between the true state of the atmosphere and the consulted forecast in the vicinity of the return height.

This relative performance is illustrated in Figure 10, presenting a minimal mean difference between the observed and modelled back azimuth. All forecasts are able to reproduce the general SSW characteristics, including the sudden reversal of the back azimuth deviation (Figure 8) as well as the sudden increase in trace velocity (Figure 9). Nevertheless, the performance skill during the SSW is significantly smaller and clearly different for all three forecast steps when compared to the summer predictions. Minimal back azimuth differences are obtained using the ten day forecast, while the nowcast yields the highest continuity of the predictions. Least performance is obtained by the five day forecast. The study of Smets et al (2016) states four important findings based on the observations at IS44 of Mount Tolbachik, sampling the local stratosphere above.

1. The warming onset (28 December 2012) is well predicted by all three forecasts, both the nowcast and five day forecast predict the same warming onset followed twelve hours later by the ten day forecast. Though, the ten day appears to be more accurate in predicting the larger back azimuth deviations and corresponding trace velocities during the first days of the warming. The resemblance in timing of the

predicted and observed stratospheric returns using the ten day forecast is better as well.

2. During the vortex displacement phase of the major warming (before 7 January 2013), the ten day forecast most accurately predicts the varying back azimuth deviation, including a sudden wind direction change around 2 January 2013 with corresponding increase in trace velocity (Figure 9). Note, that the difference in back azimuth prediction of both the nowcast and ten day forecast is below the array uncertainty. Yet, the large difference of the five day forecast when compared to the nowcast and ten day forecast is remarkable.
3. When the vortex splits (around 7 January 2013) the ten day forecast does no longer predict stratospheric returns, while the five day forecast and nowcast continue respectively two and four days with a quasi similar back azimuth difference.
4. All forecasts have difficulties to predict the stratospheric observations up to the expected warming recovery (16 January 2013). Predictions for all forecast steps indicate a too early recovery. The ten day forecast predicts a difference of about nine days with respect to the moment that no stratospheric arrivals are expected anymore (8 January 2016). The recovery is best captured by the nowcast model, continuously predicting up to 11 January 2013.

To understand the differences in performance between the forecasts, it is important to establish that the nowcast is most constrained by the data assimilation whereas the ten day forecast tends to be quasi free running, with the five day forecast positioned somewhere in between. For a typical forecast, more forecast skill is expected for a shorter forecast step, as it is closer to the data assimilation. This is observed during summer (Figure 10), where the nowcast performs best. Surprisingly, in winter the ten day forecast appears to be most accurate in predicting the first phase of the warming. Our interpretation is that the ten day forecast is able to obtain sufficient information from the small a priori warming signatures with enough time to propagate through the atmosphere, to predict the warming including the sudden recovery around 2 January 2013. Once data has to be assimilated during the warming, the ten day forecast loses a lot of forecast skill. At this stage, data gets most likely rejected or modified by the data assimilation system leading to inaccurate initialisation as addressed by (Diamantakis, 2014). The nowcast is affected similarly, but recovers approximately at once with the data assimilation system such that it predicts best the SSW duration and recovery.

Broadening the view on the arctic stratosphere, by incorporating ambient noise observations of IS18 and IS53 as introduced by Smets and Evers (2014, see Subsection 4.5), gives a different perception of the warming offset. Figure 11 shows the amplitude variations during the 2013 SSW. Observations at IS44 of Mount Tolbachik sample a regional part of the stratosphere, while the ambient noise crosses thousands of kilometers. This is of importance in stating the general onset and offset of the warming. Figure 11 indicates a somewhat later warming onset (1 January 2013). More important is the recovery. Both IS18 and IS53 point to a regular midwinter ducting around 11 January, which agrees with simulations using the nowcast. Note the gap around 7 January in Figure 11d and the diurnal phase shift, indicative for a split of the stratospheric vortex.

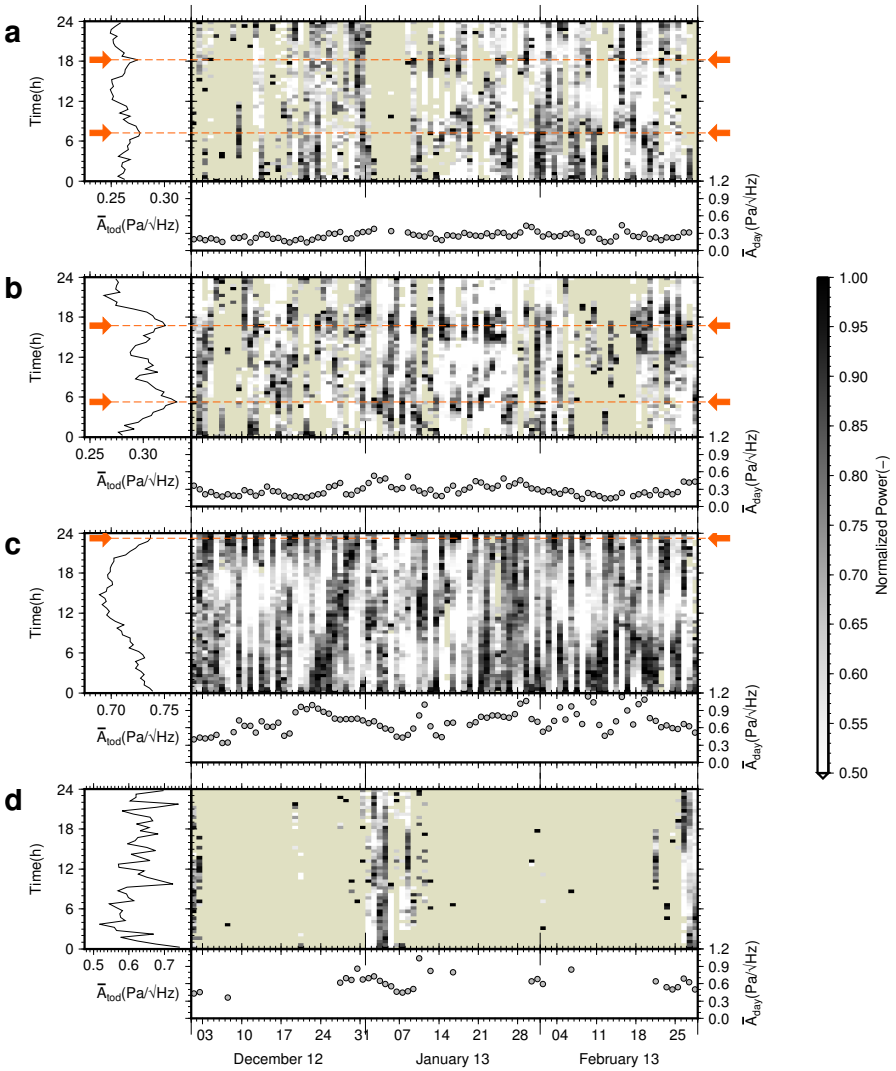

Fig. 11 Directional time averaged spectral amplitude variations for the 2013 winter (Smets and Evers, 2014). From top to bottom are shown, IS18 in direction of the Pacific Ocean (a) and Atlantic Ocean (b), IS53 in direction of the Pacific Ocean (c) and Atlantic Ocean (d), respectively. Each subfigure consists of a vertical graph (left) and an image (right) with below one horizontal graph and one colour coded bar. The vertical graph (left) shows the spectral amplitude averaged per time of day for each half hour. The red arrows and dashed lines indicate the tidal peaks in the mean time of day amplitude, if present. The image (right) shows the half hour averaged spectral power, normalised per day. The horizontal graph shows the daily mean spectral amplitude. Only detections are used with SNR $\geq$ 1.5 for IS18 and SNR $\geq$ 1.3 for IS53.

5 Outlook

Infrasound has a long history in monitoring SSWs. Several pioneering studies have focused on the various effects of a major warming on the propagation of infrasound. A clear transition can be denoted from observing anomalous signatures towards the use of these signals to study anomalies in atmospheric specifications. The typical infrasonic signature of a warming are the odd summer-like conditions in midwinter characterised by a significant change in direction of the observed infrasound (Donn and Rind, 1972; Evers and Siegmund, 2009), a change in amplitude of the ambient coherent infrasound noise (Rind and Donn, 1978), and the existence of small stratospheric shadow zones due to a hot stratosphere (Evers et al, 2012). More subtil changes are denotable during a minor warming, recognisable by the presence of a bidirectional stratospheric duct (Assink et al, 2014). The observed reduction in anisotropy is a measure for weakening of the stratospheric vortex during a minor warming. A general view of stratospheric polar vortex during a SSW is obtained by a combined analysis of all signal characteristic to unravel the stratospheric structure during a SSW (Smets and Evers, 2014). This method allow to estimate the return height from the amplitude variations, which provides detailed information on the life cycle of a warming. For the first time, differences between infrasound observations and the best deterministic state of the atmosphere (analysis) related to a SSW are indicated. Comparison of regional volcano infrasound with simulations, using various forecast steps, indicate interesting variations in stratospheric skill (Smets et al, 2016). The onset of the warming is better predicted by the 10 day forecast and duration by the nowcast. However, it is crucial to mention that the combination of infrasound observations and atmospheric models is essential in the study of SSWs.

In a next step, the method of Smets et al (2016) for the evaluation of middle atmospheric weather forecasts using near-continuous infrasound detections can directly be applied to similar setups, making use of other IMS or even national infrasound arrays. The demonstrated forecast evaluation method relies on an active volcano. However, the same methodology can be applied to ambient noise, using microbarom source predictions. In addition, source-independent techniques are being developed based on interferometry of the ambient noise field (Fricke et al, 2013, 2014). It is shown that infrasound is capable to provide detailed insight in the state of the atmosphere, of great value during a SSW. Nevertheless, it is essential to evolve towards a global comprehensive signature. Expanding towards ambient noise observations provides the ability to probe larger parts of the stratosphere. This is highly important for NWP, since improved knowledge of the global stratosphere induces a gain in tropospheric forecast skill but only when incorporating global observation (see Chapter **??** Chris Lee). Maybe in the future infrasound can assist AMSU-A observations to force the first-guess field more toward the actual state of the rapidly varying atmosphere.

Acknowledgements This research is part of the Atmospheric Dynamics Research Infrastructure in Europe (ARISE) project, funded by the European Unions Seventh Framework Program. Figures in this chapter were made with the Generic Mapping Tools (Wessel and Smith, 1991).

References

Assink JD, Waxler R, Drob D (2012) On the sensitivity of infrasonic traveltimes in the equatorial region to the atmospheric tides. J Geophys Res 117:D01,110+

Assink JD, Waxler R, Frazier WG, Lonzaga J (2013) The estimation of upper atmospheric wind model updates from infrasound data. J Geophys Res Atmos 118:10,707–10,724, DOI 10.1002/jgrd.50833

Assink JD, Pichon AL, Blanc E, Kallel M, Khemiri L (2014) Evaluation of wind and temperature profiles from ECMWF analysis on two hemispheres using volcanic infrasound. J Geophys Res 119(14):8659–8683, DOI 10.1002/2014jd021632

Assink JD, Averbuch G, Smets PSM, Evers LG (2016) On the infrasound detected from the 2013 and 2016 DPRK's underground nuclear tests. Geophys Res Lett 43(7):2016GL068,497–3533, DOI 10.1002/2016gl068497

Baldwin MP, Dunkerton TJ (2001) Stratospheric Harbingers of Anomalous Weather Regimes. Science 294:581–584, DOI 10.1126/science.1063315

Brekhovskikh IM, Goncharov VV, Kurtepov VM, Naugol'nykh KA (1973) The radiation of infrasound into the atmosphere by surface waves in the ocean. J Fluid Mech 9

Brekhovskikh LM, Godin OA (1999) Acoustics of Layered Media II: Point Sources and Bounded Beams, Springer Series on Wave Phenomena, vol 10, 2nd edn. Springer, Berlin

Chao WC (1985) Sudden Stratospheric Warmings as Catastrophes. J Atmos Sci 42:1631–1646

Charlton AJ, Polvani LM (2007) A new look at stratospheric sudden warmings. Part I: Climatology and modeling benchmarks. J Climate 20:449–469

Charlton AJ, O'neill A, Lahoz WA, Massacand AC (2004) Sensitivity of tropospheric forecasts to stratospheric initial conditions. QJR Meteorol Soc 130(600):1771–1792, DOI 10.1256/qj.03.167

Charlton-Perez AJ, Baldwin MP, Birner T, Black RX, Butler AH, Calvo N, Davis NA, Gerber EP, Gillett N, Hardiman S, Kim J, Krüger K, Lee YY, Manzini E, McDaniel BA, Polvani L, Reichler T, Shaw TA, Sigmond M, Son SW, Toohey M, Wilcox L, Yoden S, Christiansen B, Lott F, Shindell D, Yukimoto S, Watanabe S (2013) On the lack of stratospheric dynamical variability in low-top versions of the CMIP5 models. J Geophys Res Atmos 118:2494–2505, DOI 10.1002/jgrd.50125

Charney JG, Drazin PG (1961) Propagation of planetary-scale disturbances from the lower into the upper atmosphere. J Geophys Res 66:83–109, DOI 10.1029/jz066i001p00083

Chunchuzov I, Kulichkov S, Perepelkin V, Popov O, Firstov P, Assink JD, Marchetti E (2015) Study of the wind velocity-layered structure in the stratosphere, mesosphere, and lower thermosphere by using infrasound probing of the atmosphere. J Geophys Res Atmos 120(17):8828–8840, DOI 10.1002/2015jd023276

Chunchuzov IP, Kulichkov SN, Popov OE, Waxler R, Assink J (2011) Infrasound scattering from atmospheric anisotropic inhomogeneities. Izv Atmos Ocean Phys 47:540–557, DOI 10.1134/s0001433811050045

Coy L, Eckermann SD, Hoppel KW, Sassi F (2011) Mesospheric Precursors to the Major Stratospheric Sudden Warming of 2009: Validation and Dynamical Attribution Using a Ground-to-Edge-of-Space Data Assimilation System. J Adv Model Earth Syst 3(4):M10,002+, DOI 10.1029/2011ms000067

Dahlman O, Mykkeltveit S, Haak H (2009) The Treaty, Springer Netherlands, Dordrecht, chap 4, pp 83–98. DOI 10.1007/978-1-4020-6885-0_4

De Angelis S, Fee D, Haney M, Schneider D (2012) Detecting hidden volcanic explosions from Mt. Cleveland Volcano, Alaska with infrasound and ground-coupled airwaves. Geophys Res Lett 39, DOI 10.1029/2012gl053635

Diamantakis M (2014) Improving ECMWF forecasts of sudden stratospheric warmings. ECMWF Newsletter 141:30–36

Donn WL, Rind D (1971) Natural Infrasound as an Atmospheric Probe. Geophys J R Astron Soc 26:111–133, DOI 10.1111/j.1365-246x.1971.tb03386.x

Donn WL, Rind D (1972) Microbaroms and the Temperature and Wind of the Upper Atmosphere. J Atmos Sci 29:156–172, DOI 10.1175/1520-0469(1972)029%3C0156:mattaw%3E2.0.co;2

Evers LG, Siegmund P (2009) Infrasonic signature of the 2009 major sudden stratospheric warming. Geophys Res Lett 36:L23,808+, DOI 10.1029/2009gl041323

Evers LG, van Geyt ARJ, Smets P, Fricke JT (2012) Anomalous infrasound propagation in a hot stratosphere and the existence of extremely small shadow zones. J Geophys Res 117:D06,120+, DOI 10.1029/2011jd017014

Fee D, Steffke A, Garces M (2010) Characterization of the 2008 Kasatochi and Okmok eruptions using remote infrasound arrays. J Geophys Res 115(D2):D00L10+, DOI 10.1029/2009jd013621

Fee D, Waxler R, Assink J, Gitterman Y, Given J, Coyne J, Mialle P, Garces M, Drob D, Kleinert D, Hofstetter R, Grenard P (2013) Overview of the 2009 and 2011 Sayarim Infrasound Calibration Experiments. J Geophys Res Atmos 118:6122–6143, DOI 10.1002/jgrd.50398

Fricke JT, Allouche NE, Simons DG, Ruigrok EN, Wapenaar K, Evers LG (2013) Infrasonic interferometry of stratospherically refracted microbaromsA numerical study. J Acoust Soc Am 134:2660, DOI 10.1121/1.4819117

Fricke JT, Evers LG, Smets PSM, Wapenaar K, Simons DG (2014) Infrasonic interferometry applied to microbaroms observed at the Large Aperture Infrasound Array in the Netherlands. J Geophys Res 119:9654–9665, DOI 10.1002/2014jd021663

Gerber EP, Orbe C, Polvani LM (2009) Stratospheric influence on the tropospheric circulation revealed by idealized ensemble forecasts. Geophys Res Lett 36:L24,801+, DOI 10.1029/2009gl040913

Godin OA (2002) An effective quiescent medium for sound propagating through an inhomogeneous, moving fluid. The Journal of the Acoustical Society of America 112(4):1269–1275, DOI 10.1121/1.1504853

Green DN, Matoza RS, Vergoz J, Le Pichon A (2012) Infrasonic propagation from the 2010 Eyjafjallajökull eruption: Investigating the influence of stratospheric solar tides. J Geophys Res 117:D21,202+, DOI 10.1029/2012jd017988

Gutenberg B (1939) The velocity of sound waves and the temperature in the stratosphere in southern California. Bull Am Meteorol Soc 20

Hasselmann K (1963) A statistical analysis of the generation of microseisms. Rev Geophys 1, DOI 10.1029/rg001i002p00177

Hedlin MAH, Drob D, Walker K, de Groot-Hedlin C (2010) A study of acoustic propagation from a large bolide in the atmosphere with a dense seismic network. J Geophys Res 115, DOI 10.1029/2010jb007669

Holton JR (2004) An Introduction to Dynamic Meteorology, 4th edn. Elsevier Academic Press, Oxford

Janssen P (2009) The Interaction of Ocean Waves and Wind, 1st edn. Cambridge University Press

Jung T, Miller MJ, Palmer TN (2010) Diagnosing the Origin of Extended-Range Forecast Errors. Mon Wea Rev 138(6):2434–2446, DOI 10.1175/2010mwr3255.1

Kodera K, Mukougawa H, Fujii A (2013) Influence of the vertical and zonal propagation of stratospheric planetary waves on tropospheric blockings. J Geophys Res 118:8333–8345, DOI 10.1002/jgrd.50650

Kulichkov SN, Chunchuzov IP, Popov OI (2010) Simulating the influence of an atmospheric fine inhomogeneous structure on long-range propagation of pulsed acoustic signals. Izv Atmos Ocean Phys 46:69–77

Labitzke K (1977) Interannual Variability of the Winter Stratosphere in the Northern Hemisphere. Mon Wea Rev 105(6):762–770, DOI 10.1175/1520-0493(1977)105%3C0762:ivotws%3E2.0.co;2

Lalande JM, Sèbe O, Landès M, Blanc-Benon P, Matoza RS, Le Pichon A, Blanc E (2012) Infrasound data inversion for atmospheric sounding. Geophys J Int 190:687–701, DOI 10.1111/j.1365-246x.2012.05518.x

Le Pichon A, Blanc E, Drob D, Lambotte S, Dessa JX, Lardy M, Bani P, Vergniolle S (2005) Infrasound monitoring of volcanoes to probe high-altitude winds. J Geophys Res 110:D13,106+, DOI 10.1029/2004jd005587

Le Pichon A, Ceranna L, Garcés M, Drob D, Millet C (2006) On using infrasound from interacting ocean swells for global continuous measurements of winds and temperature in the stratosphere. J Geophys Res 111, DOI 10.1029/2005jd006690

Le Pichon A, Vergoz J, Herry P, Ceranna L (2008) Analyzing the detection capability of infrasound arrays in Central Europe. J Geophys Res 113(D12):D12,115+, DOI 10.1029/2007jd009509

Le Pichon A, Vergoz J, Blanc E, Guilbert J, Ceranna L, Evers L, Brachet N (2009) Assessing the performance of the International Monitoring System's infrasound network: Geographical coverage and temporal variabilities. J Geophys Res 114:D08,112+, DOI 10.1029/2008jd010907

Le Pichon A, Blanc E, Hauchecorne A (eds) (2010) Infrasound Monitoring for Atmospheric Studies, 1st edn. Springer Netherlands, Dordrecht

Le Pichon A, Assink JD, Heinrich P, Blanc E, Charlton-Perez A, Lee CF, Keckhut P, Hauchecorne A, Rüfenacht R, Kämpfer N, Drob DP, Smets PSM, Evers LG, Ceranna L, Pilger C, Ross O, Claud C (2015) Comparison of co-located independent ground-based middle atmospheric wind and temperature

measurements with numerical weather prediction models. J Geophys Res Atmos 120(16):2015JD023,273–8331, DOI 10.1002/2015jd023273

Limpasuvan V, Thompson DWJ, Hartmann DL (2004) The Life Cycle of the Northern Hemisphere Sudden Stratospheric Warmings. J Clim 17

Limpasuvan V, Hartmann DL, Thompson DWJ, Jeev K, Yung YL (2005) Stratosphere-troposphere evolution during polar vortex intensification. J Geophys Res 110, DOI 10.1029/2005jd006302

Lindzen SR, Chapman S (1969) Atmospheric Tides. Space Sci Rev 10:3–188

Longuet-Higgins MS (1950) A theory of the origin of microseisms. Phil Trans R Soc A 243:1–35

Marchetti E, Ripepe M, Delle Donne D, Genco R, Finizola A, Garaebiti E (2013) Blast waves from violent explosive activity at Yasur Volcano, Vanuatu. Geophys Res Lett 40(22):2013GL057,900+, DOI 10.1002/2013gl057900

Matoza RS, Vergoz J, Le Pichon A, Ceranna L, Green DN, Evers LG, Ripepe M, Campus P, Liszka L, Kvaerna T, Kjartansson E, Höskuldsson A (2011) Long-range acoustic observations of the Eyjafjallajökull eruption, Iceland, AprilMay 2010. Geophys Res Lett 38(6):L06,308+, DOI 10.1029/2011gl047019

Matsuno T (1971) A Dynamical Model of the Stratospheric Sudden Warming. J Atmos Sci 28:1479–1494, DOI 10.1175/1520-0469(1971)028%3C1479:admots%3E2.0.co;2

Muench HS (1965) On the Dynamics of the Wintertime Stratosphere Circulation. J Atmos Sci 22:349–360, DOI 10.1175/1520-0469(1965)022%3C0349:otdotw%3E2.0.co;2

Pierce AD (1981) Acoustics - An Introduction to Its Physical Principles and Applications. McGraw-Hill Series in Mechanical Engineering, McGraw-Hill, New York

Posmentier ES (1967) A Theory of Microbaroms. Geophys J Roy Astron Soc 13, DOI 10.1111/j.1365-246x.1967.tb02301.x

Randel W, Udelhofen P, Fleming E, Geller M, Gelman M, Hamilton K, Karoly D, Ortland D, Pawson S, Swinbank R, Wu F, Baldwin M, Chanin ML, Keckhut P, Labitzke K, Remsberg E, Simmons A, Wu D (2004) The SPARC Intercomparison of Middle-Atmosphere Climatologies. J Climate 17:986–1003, DOI 10.1175/1520-0442(2004)017%3C0986:tsiomc%3E2.0.co;2

Revelle DO (2010) Modified ray-mode (phase) theory: Understanding counter-wind propagation effects from atmospheric explosions. J Atmos Sol-Terr Phys 72:241–261, DOI 10.1016/j.jastp.2009.11.017

Rind D, Donn WL (1975) Further Use of Natural Infrasound as a Continuous Monitor of the Upper Atmosphere. J Atmos Sci 32:1694–1704, DOI 10.1175/1520-0469(1975)032%3C1694:fuonia%3E2.0.co;2

Rind D, Donn WL, Dede E (1973) Upper Air Wind Speeds Calculated from Observations of Natural Infrasound. J Atmos Sci 30:1726–1729, DOI 10.1175/1520-0469(1973)030%3C1726:uawscf%3E2.0.co;2

Rind DH, Donn WL (1978) Infrasound Observations of Variability During Stratospheric Warmings. J Atmos Sci 35:546–553, DOI 10.1175/1520-0469(1978)035%3C0546:ioovds%3E2.0.co;2

Roff G, Thompson DWJ, Hendon H (2011) Does increasing model stratospheric resolution improve extended-range forecast skill? Geophys Res Lett 38(5):L05,809+, DOI 10.1029/2010gl046515

Shaw TA, Shepherd TG (2008) Raising the roof. Nature Geosci 1:12–13, DOI 10.1038/ngeo.2007.53

Sigmond M, Scinocca JF, Kharin VV, Shepherd TG (2013) Enhanced seasonal forecast skill following stratospheric sudden warmings. Nature Geoscience 6:98–102, DOI 10.1038/ngeo1698

Smets PSM, Evers LG (2014) The life cycle of a sudden stratospheric warming from infrasonic ambient noise observations. J Geophys Res 119:12,084–12,099, DOI 10.1002/2014jd021905

Smets PSM, Evers LG, Näsholm SP, Gibbons SJ (2015) Probabilistic infrasound propagation using realistic atmospheric perturbations. Geophys Res Lett 42(15):2015GL064,992–6517, DOI 10.1002/2015gl064992

Smets PSM, Assink JD, Le Pichon A, Evers LG (2016) ECMWF SSW forecast evaluation using infrasound. J Geophys Res Atmos 121(9):2015JD024,251–4650, DOI 10.1002/2015jd024251

Stopa JE, Cheung KF, Garcés MA, Badger N (2012) Atmospheric infrasound from nonlinear wave interactions during Hurricanes Felicia and Neki of 2009. J Geophys Res 117, DOI 10.1029/2012jc008257

Sutherland LC, Bass HE (2004) Atmospheric absorption in the atmosphere up to 160 km. J Acoust Soc Am 115:1012–1032

Tailpied D, Le Pichon A, Marchetti E, Assink J, Vergniolle S (2017) Assessing and optimizing the performance of infrasound networks to monitor volcanic eruptions. Geophysical Journal International 208(1):437–448, DOI 10.1093/gji/ggw400

Tripathi OP, Baldwin M, Charlton-Perez A, Charron M, Eckermann SD, Gerber E, Harrison RG, Jackson DR, Kim BM, Kuroda Y, Lang A, Mahmood S, Mizuta R, Roff G, Sigmond M, Son SW (2014) The predictability of the extratropical stratosphere on monthly time-scales and its impact on the skill of tropospheric forecasts. QJR Meteorol Soc 141(689), DOI 10.1002/qj.2432

Tripathi OP, Charlton-Perez A, Sigmond M, Vitart F (2015) Enhanced long-range forecast skill in boreal winter following stratospheric strong vortex conditions. Environmental Research Letters 10(10):104,007+, DOI 10.1088/1748-9326/10/10/104007

Walker KT (2012) Evaluating the opposing wave interaction hypothesis for the generation of microbaroms in the eastern North Pacific. J Geophys Res 117, DOI 10.1029/2012jc008409

Waxler R, Gilbert KE (2006) The radiation of atmospheric microbaroms by ocean waves. J Acoust Soc Am 119

Waxler R, Gilbert K, Talmadge C, Hetzer C (2007) The effects of the finite depth of the ocean on microbarom signals. In: 8th International Conference on Theoretical and Computational Acoustics (ICTCA), Crete, Greece

Wessel P, Smith WHF (1991) Free software helps map and display data. Eos Trans AGU 72:441–446, DOI 10.1029/90eo00319

Whitaker RW, Mutschlecner JP (2008) A comparison of infrasound signals refracted from stratospheric and thermospheric altitudes. J Geophys Res 113:D08,117+, DOI 10.1029/2007jd008852